Mon. Not. R. Astron. Soc. **383,** 2–10 (2008) doi:10.1111/j.1365-2966.2007.12524.x

Comparative study between *N*-body and Fokker–Planck simulations for rotating star clusters – I. Equal-mass system

Eunhyeuk Kim,[1⋆] Ilsang Yoon,[1,2] Hyung Mok Lee[1] and Rainer Spurzem[3]

[1] *FPRD, Department of Physics and Astronomy, Seoul National University, Seoul 151-742, Korea*
[2] *Department of Astronomy, University of Massachusetts, Amherst, MA 01002, USA*
[3] *Astronomische Rechen-Institut, Zentr. Astron. Univ. Heidelberg (ZAH), Monchhofstrasse 12-14, 69120 Heidelberg, Germany*

Accepted 2007 September 28. Received 2007 September 27; in original form 2007 July 13

ABSTRACT

We have carried out *N*-body simulations for rotating star clusters with equal mass and compared the results with Fokker–Planck models. These two different approaches are found to produce fairly similar results, although there are some differences with regard to the detailed aspects. We confirmed the acceleration of the core collapse of a cluster due to an initial non-zero angular momentum and found a similar evolutionary trend in the central density and velocity dispersion in both simulations. The degree of acceleration depends on the initial angular momentum. Angular momentum is being lost from the cluster due to the evaporation of stars with a large angular momentum on a relaxation time-scale.

Key words: celestial mechanics, stellar dynamics – globular clusters: general.

1 INTRODUCTION

There are two different approaches to study the dynamical evolution of collisional stellar systems (e.g. globular clusters): a statistical approach and direct integration of the *N*-body equations of motion. Among the statistical methods, the Fokker–Planck (henceforth referred to as FP) equation, which is a second-order approximation of the collisional Boltzmann equation, has been frequently used. The FP equation is solved by using either Monte Carlo techniques (e.g. the series of eight papers, from Spitzer & Hart 1971 to Spitzer & Mathieu 1980, see also an alternative approach by Hénon 1971, and for recent adaptations Giersz 1998; Joshi, Rasio & Portegies Zwart 2000; Freitag & Benz 2001), or the direct numerical solution of the discretized FP equation on a mesh. In this paper, we focus on the latter approach. One-dimensional FP models assuming a spherical symmetry and isotropic velocity dispersion have been extensively exploited during the last several decades, and they have successfully elucidated the full dynamical history of star clusters (Cohn 1980; Drukier, Fahlman & Richer 1992). Two-dimensional anisotropic models are a generalization of the one-dimensional model, in which the anisotropy of the velocity dispersion between the radial and the tangential directions is taken into account; however, the isotropized distribution function continues to be used for determining the diffusion coefficients (e.g. Takahashi 1995, 1996, 1997).

The statistical methods have to make several simplifying approximations and have some limitations. More realistic simulations can be performed by directly integrating the complete equations of motion of all stars. However, the *N*-body integration still requires a huge amount of computing power. An improvement in computing facilities, particularly the advent of special purpose hardware such as GRAPE machines (Makino & Taiji 1998; Makino et al. 2003; Fukushige, Makino & Kawai 2005), made it possible to perform high-accuracy *N*-body simulations with one million body (Makino & Funato 2004; Berczik et al. 2006; Iwasawa, Funato & Makino 2006; Harfst et al. 2007). The comparisons between the results obtained from one- or two-dimensional FP models and direct *N*-body models generally show good agreement (e.g. Spurzem & Aarseth 1996). Comparative studies that use the currently available *N*-body solver for studying the dynamical evolution of collisional stellar systems are very important for checking the validity and limitations of the statistical methods. There have been several previous researches involving comparative studies (Giersz & Heggie 1994a,b, 1997; Giersz & Spurzem 1994; Freitag, Rasio & Baumgardt 2006; Khalisi, Amaro-Seoane & Spurzem 2007) and the comparisons show that for isolated non-rotating star clusters the results of FP simulations are generally in good agreement with those of *N*-body simulations. However, when a tidal boundary is included, a discrepancy between the *N*-body and FP models arises; this discrepancy becomes sensitive to *N* because the relaxation and crossing time-scales are related to different dynamical processes (Takahashi & Portegies Zwart 1998; Takahashi & Lee 2000; Baumgardt 2001). For example, the treatment of the tidal boundary has to be performed carefully in FP models since the mass evaporation process involves both orbital dynamics and two-body relaxation. The *N*-body model has to imitate the FP technique to remove stars immediately if they acquire an energy higher than the tidal energy; with these precautions, good agreement can be obtained (Spurzem et al. 2005).

Another extension of the one-dimensional FP model was carried out to include the effects of rotation. The first numerical

⋆E-mail: ekim@astro.snu.ac.kr

simulation of FP models for rotating clusters was pioneered by Goodman (1983), but neither the results nor the code was published. A more detailed and extended work by Einsel & Spurzem (1999, henceforth referred to as Paper I), who developed a new two-dimensional FP code named 'FOPAX' for this study from scratch, revealed that rotating clusters collapse faster than non-rotating ones. A post-core collapse study of rotating star clusters, improving 'FOPAX' by several features, including an energy source due to formation and hardening of three-body binaries, was done later by Kim et al. (2002, henceforth referred to as Paper II). Papers I and II studied the dynamical evolution of rotating stellar systems using the orbit-averaged two-dimensional FP equations only for equal-mass systems. In both cases and in the study of Goodman (1983), it was assumed that the distribution function f depends only on the energy and z-component of the angular momentum (J_z). Kim, Lee & Spurzem (2004, henceforce referred as Paper III) extended the method to multi-mass systems, and exhibit interesting results concerning the segregation of mass and angular velocity with heavy stars in the cluster centres. Fiestas et al. (2006) modelled individual rotating globular clusters using the model, and Fiestas & Spurzem (in preparation) included a star-accreting central black hole with a loss cone. In general, according to the strong Jeans theorem there are three integrals of motion with regard to the orbital motion of stars in axisymmetric potentials (Binney & Tremaine 1987). Two of the integrals of motion are known as E and J_z. However, the nature of the third integral of motion is not known clearly. In addition to the standard approximation required for FP models, the two-dimensional FP models presented here and in Papers I–III ignore any effect of the third integral. For stellar systems not too much flattened, it might be possible to construct three-dimensional FP models following the three integral models of Lupton & Gunn (1987), in which the square of total angular momentum (J^2) was adopted as an approximate third integral. However, it would be an extremely difficult task numerically and physically (owing to the diffusion coefficients!); even then it would still be approximate since we do not know the third integral analytically (cf. Binney & Tremaine 1987 regarding this issue). Hence, a thorough comparison with direct N-body models appears to be the best method to acquire knowledge on the validity of all approximations made in our two-dimensional FP models.

There have been some preliminary studies of rotating star clusters involving comparisons between N-body and FP methods (Boily 2000; Boily & Spurzem 2000; Ardi, Mineshige & Spurzem 2005; Ernst et al. 2007). Although these authors found good agreements between these two methods, the number of cases studied is rather limited. This can be understood in two ways. First, for a smaller value of N (say up to a few 10^4) a large number of statistically independent simulations are needed, and only the ensemble average can be compared with the approximate FP models. On the other hand, different physical models, such as isolated or tidally limited models, different degrees of central concentrations of stars (i.e. different central potential), need to be studied. In this paper, we have carried out a series of numerical N-body simulations of rotating stellar systems, which are directly comparable with our two-dimensional FP models in Papers I and II. By comparing the results with those obtained from FP models, we can investigate the validity of the assumptions made in rotating FP models.

This paper is organized as follows. In the next section, we briefly describe initial N-body models and compare them with FP models. In Section 3, we present the numerical results obtained from N-body simulations and their comparisons with those of FP models. The summary and discussions are given in the last section.

2 THE MODELS

2.1 Numerical methods

The FP code FOPAX, which takes into account the effect of rotation, was developed in Papers I–III in order to study the secular evolution of star clusters having initial rotation.

For performing direct N-body simulations to study the dynamical evolution of rotating stellar systems, we have used the currently available high-accuracy, collisional N-body code NBODY6 (Aarseth 1999). The NBODY6 code uses the fourth-order Hermite scheme with hierarchical block time-steps (HTSs) and the Ahmad–Cohen neighbour scheme for particle integration. Close encounters between stars and persistent binaries formed by three-body interactions are solved for their internal motion by using two-body regularization methods (Kustaanheimo & Stiefel 1965) and chain regularization (Mikkola & Aarseth 1990, 1993, 1996, 1998). Although NBODY6 is capable of dealing with many more astrophysical components such as the existence of primordial binaries and stellar mass loss due to stellar evolution, we have considered only the treatment of close encounters between stars in this study since we are mainly interested in the role of the initial angular momentum on cluster dynamics and in comparisons with FP simulations.

2.2 Initial models and boundary condition

In Paper II, the initial two-dimensional FP models are generated according to Lupton & Gunn (1987). Our initial N-body models that follow rotating King models with a central concentration of $W_0 = 6$ have the same conditions as those of two-dimensional FP models in Paper II. We have constructed the initial models for the N-body simulations from the two-dimensional FP models in Paper II by random number generation. Three different initial rotations ($\omega_0 = 0.0$, 0.3 and 0.6) are considered in this work. In Table 1, we list some information on the initial models used for the present simulations.

Since most globular clusters are bound to their host galaxy, they are tidally limited and stars escape from them through a tidal boundary. There are many previous studies that considered the effects of the tidal field on cluster evolution and comprehended it as an important component of the evolution (e.g. Lee & Ostriker 1987; Lee & Goodman 1995; Takahashi & Portegies Zwart 1998; Takahashi & Lee 2000; Yim & Lee 2002; Spurzem et al. 2005; Lee, Lee & Sung 2006). Among the few different implementations of modelling the tidal effects, we adopted the instantaneous removal of stars whose total energy exceeded tidal energy of the cluster. This approximation is known to be inconsistent with the realistic N-body treatment for small-N models, but the inconsistency decreases for a large value of N. We considered the equal-mass models, which are tidally bound to their host galaxy, in order to compare the obtained results with the FP results in Paper II. We have modified the original NBODY6 code to imitate the tidal environment of the clusters modelled with the two-dimensional FP equation in Paper II; this implies that we promptly

Table 1. Initial parameters for the equal-mass models.

W_0	ω_0	r_t/r_c	r_h/r_t	$T_{tot}/\|W\|^a$	N
6	0.0	18.0	0.15	0.000	10 240
	0.3	14.5	0.18	0.035	10 240
	0.6	9.6	0.24	0.101	10 240

[a] $T_{tot}/|W|$: ratio of rotational energy to potential energy.

remove stars whose energies exceed the tidal energy ($e > e_{\rm tid}$, see equation 1), as considered in two-dimensional FP models. In order to maintain the density within the tidal radius constant, the tidal radius decreases with time when there is a loss of mass through the boundary. Subsequently, we have adjusted the tidal energy at every regular time-step according to the following expression:

$$e_{\rm tid}\,(t) = -\frac{GM(t)}{r_{\rm tid}}, \qquad (1)$$

where $r_{\rm tid}$ and $M(t)$ are the tidal radius and the total mass of the cluster within the tidal radius, respectively. We have used the initial tidal radius obtained from the FP models to compute the mean density that is kept constant.

The number of stars (N) in a cluster is one of the important parameters for the dynamical evolution of the cluster. While the computational burden (except for the core-collapse phase) does not significantly depend on N in the statistical FP method, the number of stars is very important in the N-body simulation as the computation time becomes nearly proportional to N^3. We use $N = 10\,240$ for the present equal-mass models only because the number should be close to that used in Paper II ($N = 5000$). In testing the validity of our FP models, it does not matter that the actual number of stars in globular clusters is significantly larger. The choice of the number of stars determines the relative strength of the three-body interactions, which initiate the post-collapse phase (see e.g. Spurzem & Aarseth 1996).

The realization of the rotating King model for N-body simulations is shown in Figs 1 and 2. We have shown the radial profiles of density for both the N-body and the FP models (Fig. 1) and the distribution of the radial and tangential velocities of the stars in the N-body realization of the rotating King models (Fig. 2). Three N-body models having different degrees of rotation are compared with the two-dimensional FP models. Each density profile is obtained from the mean of 10 different initial models generated by different random seed numbers. The open circles represent the density profile adopted in the FP models. Each $r_{\rm tid,0}$ is the initial tidal radius derived from the FP model. Excellent agreement is observed

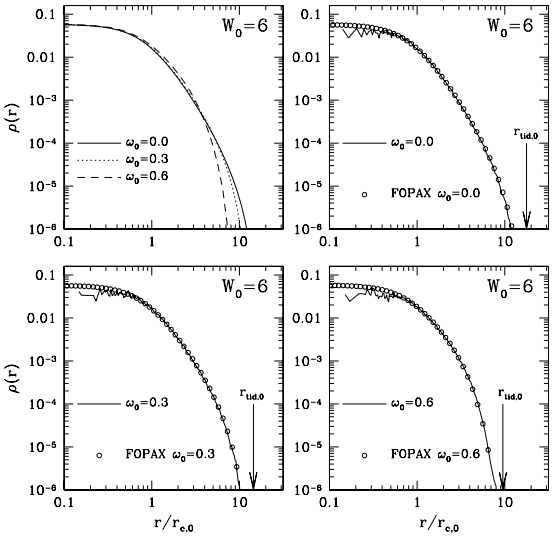

Figure 1. Radial profiles of the density for the initial N-body models with a central potential of $W_0 = 6$ and $\omega_0 = 0.0, 0.3$ and 0.6. The upper left-hand panel shows the FOPAX results. For comparison, the density profile of the initial FP model with $(W_0, \omega_0) = (6, 0.6), (6, 0.3)$ and $(6, 0.0)$ is shown (open circles). The N-body realization of the initial model shows good agreement with that of the FP model, except for the central region.

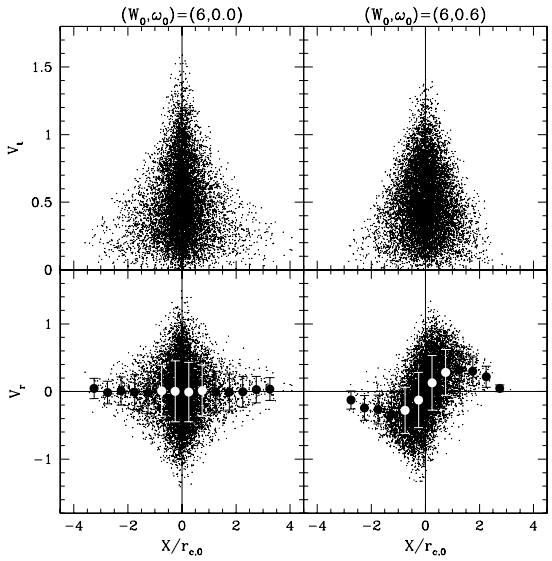

Figure 2. Tangential and radial velocity distributions of the initial N-body models with a central potential of $W_0 = 6$ and initial rotation of $\omega_0 = 0.0$ (left-hand panels) and 0.6 (right-hand panels). The X-axis represents the sky-projected equatorial distance measured in units of the initial core radius. The mean radial velocity distribution along the projected equator is shown by the filled circles with 1σ errors. The central solid body rotation and the subsequent highly differential rotation are typical of rotating clusters (see fig. 10 of Paper II for comparison).

between the radial profile beyond the core radius ($r_{\rm c}$) in the N-body realization and that in the FP model. However, within $r_{\rm c}$, the density of the N-body model is slightly lower than that of FP model. This may be due to the fact that the number of stars inside the core is rather small. However, due to inevitable random fluctuations, it is impossible to construct initial N-body models perfectly identical to the FP models. We believe that statistical FP models agree very well with the averaged N-body models and increasing the number of stars will improve the degree of agreement. Fig. 1 also shows that increasing the rotation decreases the concentration of the stellar system (smaller ratio between the tidal and the core radii).

The position–velocity distributions that are sky-projected are displayed in Fig. 2 for the N-body models of non-rotating ($\omega_0 = 0.0$, left-hand panels) and highly rotating ($\omega_0 = 0.6$, right-hand panels) clusters with the central potential of $W_0 = 6$. To have maximum effect of initial rotation in sky-projected distribution, we project the model clusters on the sky in such a way that the rotating axis is a perpendicular axis in the sky-projected plane. The distance to the rotation axis is measured in units of the initial core radius. We also show the mean profiles of the radial velocities with 1σ errors (filled circles). The profile of the radial velocity for the non-rotating model shows increasing velocity dispersion towards the centre of the cluster. A typical velocity structure of the rotating model is shown clearly in the distribution of the radial velocities of the rotating model: rigid-body rotation inside the core radius and highly differential rotation subsequently.

3 RESULTS

3.1 Core collapse, central density, and central velocity dispersion

We start the discussions by presenting the results for the evolution of the central density and central velocity dispersion (Fig. 3). The

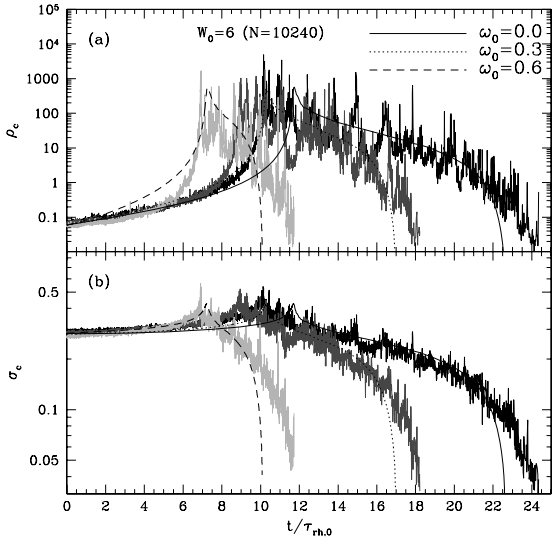

Figure 3. Evolution of central density and central velocity dispersion for each model. FOPAX models are shown with the smooth lines.

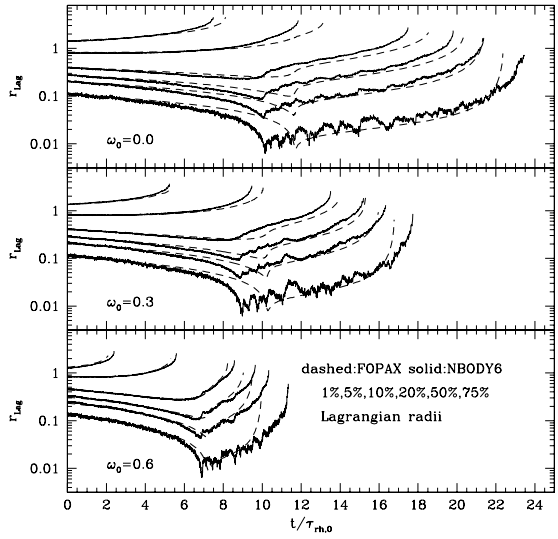

Figure 4. Time-evolutions of the Lagrangian radii containing 1, 5, 10, 20, 50 and 75 per cent of the initial cluster mass. The initial parameters that characterize the cluster model are written on the lower left-hand corner of each panel. The FOPAX calculations are shown with the dashed lines on each panel.

Table 2. Time-scales of tidally bound models.

Model	W_0	ω_0	$t_{\rm cc}$ [$\tau_{\rm rh,0}$]	$t_{\rm dis}$ [$\tau_{\rm rh,0}$]	$M_{\rm cc}$
		0.0	10.1	24.30	0.63
N-body	6	0.3	8.7	17.75	0.55
		0.6	6.9	11.55	0.37
		0.0	11.73	22.61	0.59
FOPAX	6	0.3	10.31	16.96	0.48
		0.6	7.27	10.08	0.33

central density increases with time due to the two-body relaxation for an equal-mass system, where the time is measured in units of initial half-mass relaxation time ($\tau_{\rm rh,0}$). The expression for $\tau_{\rm rh,0}$ for the equal-mass system is given by the following formula (Spitzer & Hart 1971):

$$\tau_{\rm rh,0} = 0.138 \frac{N^{1/2} r_{\rm h,0}^{3/2}}{G^{1/2} m^{1/2} \ln\Lambda}, \quad (2)$$

where $N, r_{\rm h,0}, G, m$ and $\ln\Lambda = \ln(\gamma N)$ denote the total number of stars, initial half-mass radius, gravitational constant, mean mass of stars and Coulomb logarithm, respectively. It has been shown by Giersz & Spurzem (1994) and Giersz & Heggie (1994a,b) that the best agreement between the direct *N*-body calculations and orbit-averaged FP equation is achieved when the coefficient γ in the Coulomb logarithm has a value of 0.11. Therefore, we use this value in this work as it is also used in Paper II. Since the half-mass radius varies with the rotation parameter ω_0, the values of $\tau_{\rm rh,0}$ could also depend on ω_0, even for models with the same W_0.

The time of core collapse ($t_{\rm cc}$), the time for the complete disruption of the cluster ($t_{\rm dis}$), and the cluster mass at the time of core collapse in units of initial cluster mass ($M_{\rm cc}$) are listed in Table 2. We can easily note that the rotating models evolve faster than the non-rotating ones, in both the *N*-body and FP models. The faster the cluster rotates, the shorter the time taken for the core collapse. As discussed in detail in Papers I and II, the acceleration is caused by the combination of gravothermal and gravogyro instabilities.

In Fig. 3, we show the evolution of the central density ($\rho_{\rm c}$) and central velocity dispersion ($\sigma_{\rm c}$) of the cluster. The results obtained from the FP and *N*-body models are displayed as the smooth lines and solid lines with a large fluctuation, respectively. Although the core collapse occurs at slightly different times (one can estimate $t_{\rm cc}$ more accurately in Fig. 4), there is good agreement between the FP and *N*-body results. The *N*-body model produces rather noisy data since there is a significant statistical fluctuation in the physical parameters. However, we can still perform some quantitative comparisons between the FP and the *N*-body approaches. In the early evolutionary stage, the central density derived from the *N*-body model is less than the value obtained by FP for the model with $\omega_0 = 0.6$. This may reflect the difficulty in determination of the central density for *N*-body models, especially for rapidly rotating clusters that are significantly flattened. Therefore, the most rapidly rotating model has the largest discrepancy with regard to the central density between the *N*-body and the FP models.

From Table 2, we note that the times for core collapse in the FP simulations are generally greater than those in the *N*-body simulations by 5–15 per cent. Apparently, different approaches should yield some different results, and we regard a small difference of 5–15 per cent in $t_{\rm cc}$ as being insignificant. These differences would decrease for large N models as the assumptions made in the FP method become more appropriate. In fact, we have observed that $t_{\rm cc}$ decreases for models with large values of N when we compared the simulations performed for *N*-body models with $N = 5000$ and 10 240.

After the core collapse, the evolutions of $\rho_{\rm c}$ derived from the *N*-body and FP models are also somewhat different from each other. Towards the end of the evolution, the difference becomes quite significant. The disruption time of the *N*-body models is slightly larger than that of the FP models. This is due to the fact that the escape rate varies with the number of stars. We perform more detailed comparisons on the evaporation of stars in Section 3.3. It is easier to determine the exact core-collapse time based on the evolution of the central velocity dispersion because the fluctuation amplitude is smaller than that of the central density. The times of core collapse listed in Table 2 are determined by inspecting the behaviour of $\sigma_{\rm c}$.

We show the evolution of the Lagrangian radii of the equal-mass models in Fig. 4. The results from the FP simulation are displayed

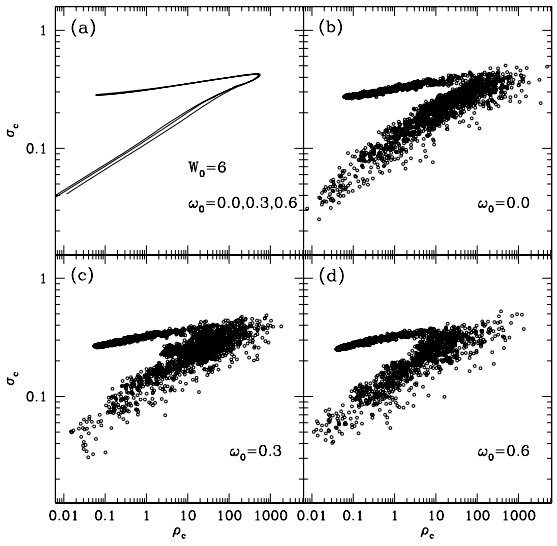

Figure 5. The evolution of σ_c as a function of ρ_c. σ_c follows power laws during pre- and post-collapse states. The evolution is nearly independent of ω_0.

by the dashed lines. Each line represents the radii where the cluster contains 1, 5, 10, 20, 50 and 75 per cent of the *initial* mass of the cluster. It is not straightforward to determine the Lagrangian radii in a flattened system. In Paper I, the Lagrangian radii were evaluated along the specific zenith angle where the effects of flattening on the mass shells are expected to be less important; the same zenith angle is used in Fig. 4. However, as our models are nearly spherical, we determine the Lagrangian radii on the assumption that the system is spherically symmetric for the *N*-body models. As seen in Fig. 4, differences between the FP and the *N*-body models are very small. Analysing in more depth, we note that after the core collapse, the inner part of the cluster expands more rapidly in the FP model than in the *N*-body model, although the difference is rather small.

The relationship between the central density and the central velocity dispersion is shown in Fig. 5. The upper left-hand panel (Fig. 5a) shows the relation between σ_c and ρ_c which is obtained from all the three FP models with different initial rotations. The other three panels (Figs 5b–d) show the results of the *N*-body models. From Papers I and II, we know that this relationship is not affected considerably by the initial rotation, as shown in Fig. 5(a). Again, we find good agreement between the FP and the *N*-body models. The large amount of scatter during the post-core collapse phase, as shown in Fig. 5 is mainly due to the large fluctuation in the central density. The power-law behaviour of σ_c on ρ_c during the pre-collapse phase is a consequence of the self-similarity of the collapsing core and it is well known that $\sigma_c \propto \rho_c^{0.1}$ during this stage (Cohn 1980). During the post-collapse phase, we can derive the relationship between σ_c and ρ_c using an energy balance argument and the assumption of self-similar evolution (see Section 3.4). It follows that $\sigma_c \propto \rho_c^{\beta}$ with $\beta = 0.25$, which is in good agreement with $\beta = 0.23$ derived from the FP model in Paper II. The *N*-body results appear to follow similar power-law behaviour, although the power-law index β is difficult to determine because of the large scatter.

From the *N*-body calculations, we have confirmed the earlier finding of a significant acceleration in cluster evolution due to rotation, which was obtained from the FP calculations in Papers I and II. We also find that both the *N*-body and FP models give similar results, although there are small differences with regard to the time of core collapse, and the disruption times.

3.2 Evolutions of anisotropy and angular momentum

In axially symmetric systems, the natural decomposition of velocity vectors is to use the cylindrical coordinate which has its origin at the centre of mass of the cluster. We investigate the evolution of the velocity dispersions (σ_R, σ_ϕ, and σ_z) and show the evolution of these quantities in Fig. 6, where (R, ϕ, z) represents the conventional axis of the cylindrical coordinate system.

For initially rotating models, these three velocity dispersions have different values. In the right-hand panels of Fig. 6, the ratio of σ_ϕ to σ_0 is initially greater than 1 for the rotating models and approaches the isotropic value of 1, where σ_0 represents the average one-dimensional velocity dispersion defined by $\sigma_0 = (\sigma_R^2 + \sigma_\phi^2 + \sigma_z^2)^{1/2}/\sqrt{3}$.

The angular momentum in rotating stellar systems is transferred outwards through two-body relaxation, and is also lost due to escaping stars. The stars gaining a large angular momentum migrate to the outer parts of the system, while those losing angular momentum drift towards the central parts. As the stars with a high angular momentum move outwards and finally escape from the cluster, the total angular momentum of the system decreases with time.

In Fig. 7, we display the evolutions of the z-component of the angular momentum per unit mass (J_z) of an entire cluster. The results from the *N*-body models are shown by the solid lines, while those from the FP models are shown by the dashed lines. To indicate the degree of error in determining J_z, we also show the time-evolution of J_z for the non-rotating model. We first note that there is good agreement between the *N*-body and FP results. The effect of neglecting the third integral in the FP models is minimized when dealing with global cluster properties (e.g. total cluster mass and total angular momentum), while this effect is severe for local properties (e.g. central density). It is clearly shown that J_z monotonically decreases with time. The loss rate of angular momentum is large in the early phases and decreases as the cluster evolves (see Fig. 7b). The combined

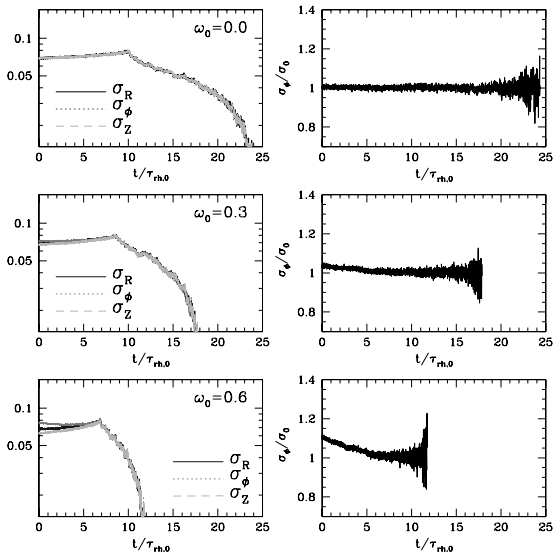

Figure 6. Time-evolutions of σ_R, σ_ϕ and σ_Z (left-hand panels) and σ_ϕ/σ_0 (right-hand panels) for each model. At the time of core collapse, σ_R, σ_ϕ and σ_Z are almost equal and $\sigma_\phi/\sigma_0 \approx 1$, where σ_0 is the one-dimensional velocity dispersion.

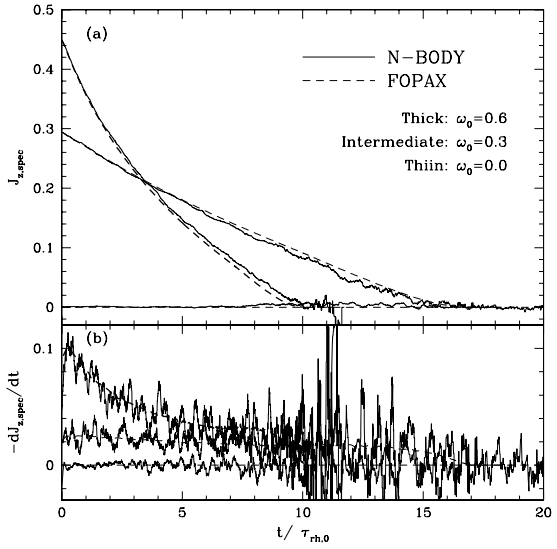

Figure 7. Evolution of the z-component of angular momentum per unit mass (J_z) (Fig. 7a) and the loss rate of J_z (Fig. 7b). The results for the N-body model and FP model are shown with the solid lines and dashed lines, respectively. The J_z evolution for the non-rotating model indicates the corresponding error in determining the J_z. It is clearly shown that J_z for rotating models decreases with time due to the escape of stars possessing an angular momentum and that the time-evolution of J_z in the N-body and FP models agrees quite well. The loss rate of J_z for the N-body models (solid lines) is smoothed for easier comparison.

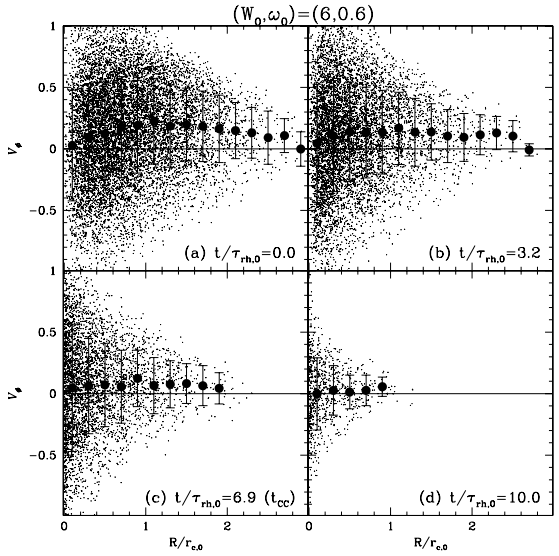

Figure 8. Distribution of the V_ϕ at four selected evolutionary epochs in a cylindrical coordinate system for a model with $(W_0, \omega_0) = (6, 0.6)$. When there is no rotation, it should show a symmetry with respect to $V_\phi = 0$. A asymmetry of V_ϕ disappears with increasing time due to the loss of the angular momentum. The filled circles are the average V_ϕ values and the error bar corresponds to 1σ dispersion.

effect of gravitation and rotation accelerates the evolution of the cluster. A substantial loss of the initial angular momentum in an entire cluster prevents rotation from playing an important role in the evolution of a cluster in later phases. Since the cluster is losing mass at a nearly constant rate, the total angular momentum of the cluster decreases more rapidly than J_z.

3.3 Evolutions of rotation curve

We can construct the rotation curves by computing the averages of V_ϕ, which is the ϕ-component of the velocity of stars. We choose the model with $\omega_0 = 0.6$ and present the distribution of V_ϕ for all stars at some specific epochs in Fig. 8. The asymmetry of V_ϕ with respect to $V_\phi = 0$ indicates the global rotation of the stellar system. During the pre-collapse phase, V_ϕ becomes more dispersive, particularly around the central region. A large spread near the centre ($R \sim 0$) at $t = t_{cc}$ and the slight asymmetry of V_ϕ indicate that the cluster is losing angular momentum; this also indicates that as the core collapse approaches, the stars are falling into the central region of the cluster with a high angular speed (but low rotation velocity). After t_{cc}, V_ϕ still has a small amount of asymmetry.

The radial profiles of the rotational velocity (v_{rot}) for the model with $\omega_0 = 0.6$ are shown in Fig. 9. We also display the radial profiles of v_{rot} obtained from the FP model by the dashed lines. The profiles at different evolutionary epochs are shown with different symbols: the filled squares for the initial model, open circles for the pre-collapse phase, filled circles at the time of core collapse, and open star marks for the post-collapse phase. The radial profiles in Fig. 9 are obtained by averaging V_ϕ for stars having the same value of R in cylindrical coordinates.

The radial profiles of v_{rot} at the initial epoch shows good agreement between the N-body and FP models except for a very central region ($R < 0.5r_c$). The amount of rotation decreases with time and

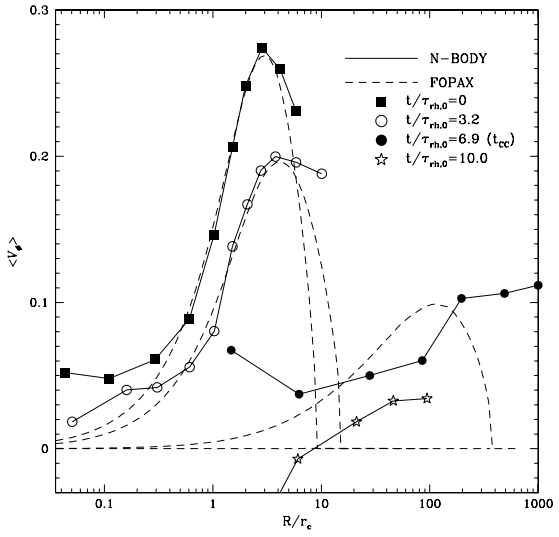

Figure 9. Radial profiles of mean rotational velocities of the cluster model with $(W_0, \omega_0) = (6, 0.6)$ at four evolutionary stages. The radii are measured in units of the current core radius (r_c). For comparison, we show the rotational profiles from the FP models by the dashed lines.

the radius where v_{rot} has the peak value progresses outwards when the radius is measured in units of the current core radius. This is a consequence of the self-similar evolution during the pre-collapse phase (Papers I and II). The radial profiles of v_{rot} for the N-body model during pre-collapse phases agree well with those for the FP model. However, at later times, the two methods yield somewhat different rotation curves. For example, at the time of core collapse, the N-body model predicts a larger rotation speed for the stars in the central and outer parts as compared to the FP method. The rotation seems to continue until a very late epoch ($t = 10t_{rh,0}$) in the N-body model, while there is virtually no rotation left in the FP model.

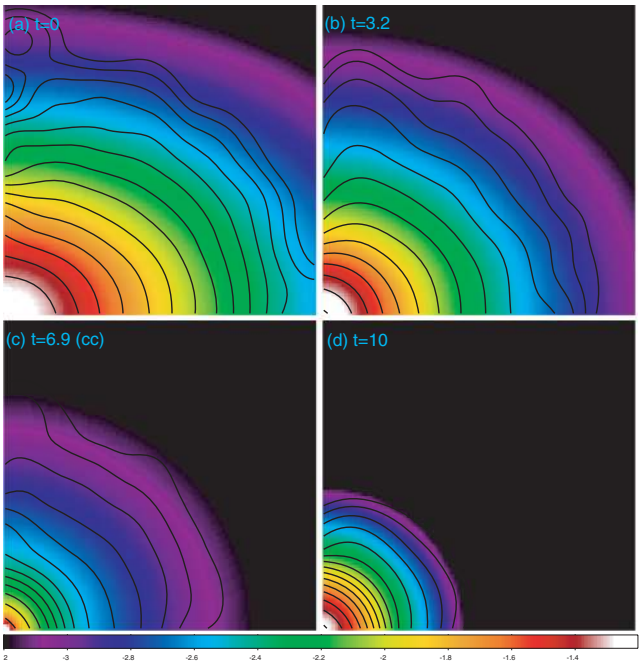

Figure 10. Density distribution of stars in (R, Z) coordinate at four selected evolutionary epochs for a model with $(W_0, \omega_0) = (6, 0.6)$ as computed by N-body (contour map) and FP methods (colour map). The horizontal axis is R running from 0 to 3 in units of the initial core radius, while the vertical axis is the z-coordinate with the same scale. The N-body and FP methods give almost the same density distribution.

In Fig. 10, we have shown the distribution of the stellar density in the form of a colour map for the FP results and in the form of iso-density contours for the N-body results. The four panels represent different epochs for the cluster with largest initial rotation speed ($\omega_0 = 0.6$). We display the cluster shapes in (R, z) coordinates because we assume that the initial model has the axis of rotation along z in cylindrical coordinates. To compare the cluster shapes at different epochs, we measure the size in units of initial core radius ($r_{c,0}$). First, we note that the shapes computed by the N-body and FP models are almost identical. As the rotation becomes negligible, the stellar system becomes more spherical. The effects of rotation on the flattened shape of a cluster are observed during the time of core collapse and the post-collapse phase (Figs 10c and d); the shape of the cluster around the central region is almost spherical.

3.4 Tidal boundary

If the cluster rotates around the host galaxy on a circular orbit, the tidal field experienced by the cluster does not change with time. In a steady tidal field, the tidal radius is expressed as follows:

$$r_{\rm tid} \approx \left(\frac{M}{3M_{\rm G}}\right)^{1/3} R_{\rm G}, \tag{3}$$

where M is the total mass of the cluster within the tidal boundary; $R_{\rm G}$, the distance of the cluster from the galactic centre; and $M_{\rm G}$, the galactic mass within $R_{\rm G}$. The above equation ensures that the mean density within the tidal radius is a constant. As the cluster loses the stars beyond the tidal boundary, the tidal radius has been adjusted to maintain a constant mean density.

We depict the evolution of the total mass of the cluster in Fig. 11. During the pre-collapse phase, the evolution of the total mass, which is computed from the N-body and FP models, is similar but shows

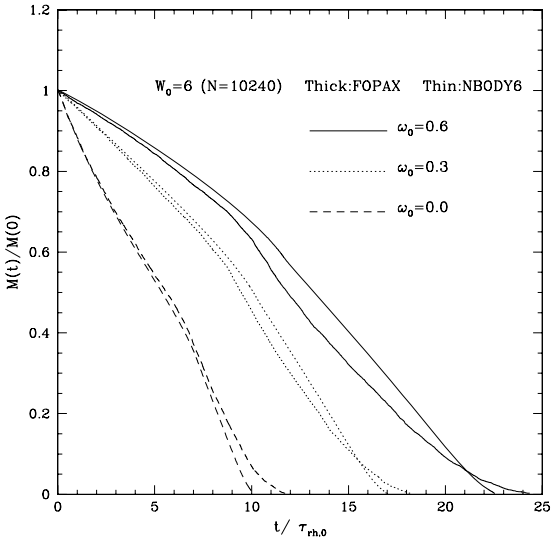

Figure 11. The evolution of the total mass of the cluster. The discrepancy between FOPAX and NBODY6 is mainly due to the number of particles after the core collapse.

small deviation from each other. However, after the core collapse, the two methods result in somewhat different behaviour. This discrepancy in post-collapse phase is partly due to the accumulation of small difference during the pre-collapse phase. The escape rate of the N-body simulation is lower than that of the FP simulation. This may be caused due to the decrease in the number of stars in the cluster. We have assumed the *instantaneous* escape of stars whose energy exceeds the tidal energy. However, in the FP simulations, the time-step is determined by the fraction of the relaxation time, while the N-body uses a time-step proportional to the *crossing time-scale*. As the cluster loses its mass, the ratio between these two time-steps changes. In other words, the crossing time-scale and the relaxation time-scale have the following relationship (Binney & Tremaine 1987):

$$t_{\rm relax} \approx \frac{0.1N}{\ln \Lambda} t_{\rm cross}. \tag{4}$$

Therefore, $t_{\rm cross}/t_{\rm relax}$ increases as N decreases. This means that the N-body simulation removes stars less effectively than the FP simulation for small values of N; this is why we observe a long tail in the N-body results in Fig. 11. In N-body simulations, after the core collapse, the number of stars remaining in the cluster is of the order of 10^3. This is not a sufficient number to obtain results comparable with the FP method. Hence, the escape rate for N-body models is lesser than that for the FP models during the late stages of the evolution and N-body models survive longer than FP models. We can also observe this effect in Fig. 3. In this figure, central density features are observed to be inconsistent between the N-body and the FP models towards the end of the evolution. With more stars, this gap would become narrower. Since the number of stars in a real globular cluster is considerably larger than that used in the present N-body simulations, the difference between N-body and FP models would decrease for a realistic number of stars (see Takahashi & Portegies Zwart 1998).

3.5 Core, half-mass, and tidal radii

We now investigate the evolution of the core, half-mass, and tidal radii of the star cluster. The behaviour of $r_{\rm tid}$ and $r_{\rm c}$ in units of the

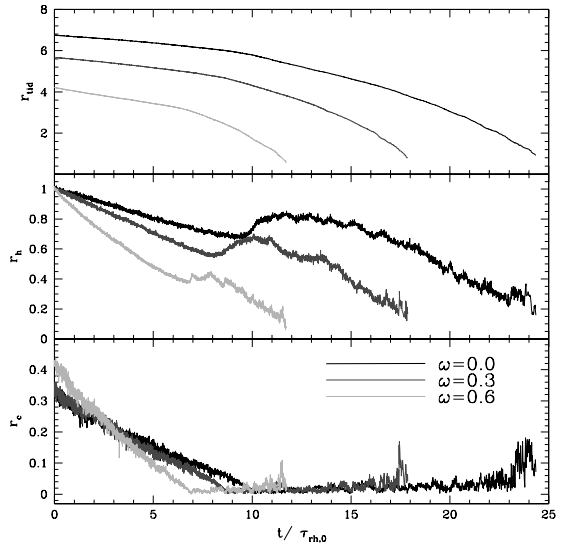

Figure 12. Time-evolution of r_c, r_h and r_{tid} measured in units of the initial half-mass radius (r_h, 0). The most rapidly rotating cluster has the largest r_c and r_h, and the smallest r_{tid}.

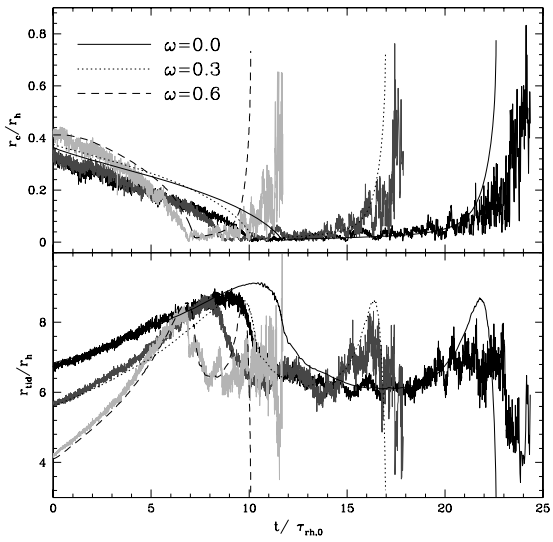

Figure 13. Time-evolution of r_c/r_h and r_{tid}/r_h. The self-similarity feature after t_{cc} is shown. In particular, the evolution of r_{tid}/r_h shows good agreement with that of FP.

initial half-mass radius ($r_{h,0}$) is shown in Fig. 12. As the rapidly rotating initial model has a half-mass radius smaller than the slowly rotating model, the initial value of r_c/r_h for the most rapidly rotating cluster is larger than that of the other two models, as shown in Fig. 13 (Paper II). The evolutions of r_c and r_{tid} in units of r_h at the same evolutionary stage as those in Fig. 12 are shown in Fig. 13. We find that there are significant differences in r_c/r_h between the FP and the *N*-body models, while the difference is not so apparent in r_{tid}/r_h. This reflects the difficulties in determining r_c for the *N*-body models with a relatively small value of *N* rather than any systematic differences in different approaches. Both r_c and r_h decrease with time, although there is a difference in the decreasing rate that depends on the initial degree of rotation. After the core collapse, both r_c and r_h increase for some time at almost the same rate due to self-similar expansion. Subsequently, the tidal boundary shrinks rapidly after core bounce. Therefore, the half-mass radius begins to decrease again. However, the shrinking of r_{tid} does not affect the central region and r_c continues to increase. At the end of the evolution, r_c shows a steep increase; this signals the complete disruption of the cluster.

After the core collapse, r_c/r_h and r_{tid}/r_h show nearly the same behaviour. The value of r_c/r_h is almost constant and the evolution of r_{tid}/r_h for different initial models is similar to each other and independent of the rotation parameter ω_0. We already have assumed the self-similar evolution of the inner part of the stellar system in order to explain the relation between ρ_c and σ_c after t_{cc} (Fig. 4). We can express $\sigma_c^2 \sim \frac{M_c}{r_c}$ and $\sigma_h^2 \sim \frac{M_h}{r_h}$, where M_c and M_h are the masses within r_c and r_h, respectively. Since the inner parts of the cluster are nearly isothermal, we obtain $\sigma_h/\sigma_c =$ constant. With the self-similarity assumption ($r_c/r_h =$ constant), we can rewrite σ_c as $\sigma_c \sim \rho_h^{1/6} M^{1/3}$. On the other hand, according to Goodman (1987), the energy balance argument predicts that $\rho_c/\rho_h \propto M^{4/3}$. Therefore, $\sigma_c \sim \rho_c^{1/4} \rho_h^{-1/12}$. If we use the tidal boundary condition, $M/r_{tid}^3 =$ constant and $\rho_h \sim \frac{M}{r_h^3}$, we can obtain the following relation:

$$\ln \sigma_c \sim \frac{1}{4} \ln \rho_c - \frac{1}{4} \ln \frac{r_{tid}}{r_h}. \quad (5)$$

The variation in $\frac{r_{tid}}{r_h}$ during the post-collapse phase is very small (by a factor of few) as compared with that in ρ_c (by a few orders of magnitude), except near the disruption time. Therefore, we can approximately write the following relation:

$$\ln \sigma_c \sim \frac{1}{4} \ln \rho_c. \quad (6)$$

If we express $\sigma_c \propto \rho_c^{\beta}$, $\beta = 0.25$, then this value is close to 0.23 that was achieved in Paper II.

4 SUMMARY AND DISCUSSION

We have performed numerical simulations for the evolution of initially rotating star clusters with equal mass using NBODY6 and have compared the results with those computed by the direct integration of the FP equation. We have considered clusters with $N = 10\,240$. For critical comparisons between *N*-body and FP models, we constructed the initial *N*-body models using the initial two-dimensional distribution function used for FP models.

We observed the acceleration of the core collapse, as reported in Papers I and II. The degree of acceleration obtained from the present *N*-body models is slightly different from that obtained from the FP models; however, the small difference in the core-collapse time between the *N*-body and statistical methods (FP model, gaseous model, etc.) has also been observed earlier (Spurzem & Aarseth 1996). The entire evolutionary trend of the central density agrees with that of the FP models.

The *z*-component of the specific angular momentum (J_z) is observed to monotonically decrease with time for the clusters with initial rotation. The global evolutionary trend of J_z between the *N*-body and the FP models shows excellent agreement. The loss rate of J_z decreases as the cluster evolves. Therefore, we conclude that during the early stages the existence of initial rotation significantly affects the entire cluster evolution.

In FP simulations, the cluster evolution will be independent of the third integral to the end of time. On the other hand, in the *N*-body simulations, the third integral effect may appear during the evolution. In addition, there is a limit on the number of stars and the random fluctuations of the *N*-body models in this study and these limits also causes differences with the FP method. Therefore, we

need to perform more *N*-body simulations with a larger number of stars or with various models by using different random numbers.

ACKNOWLEDGMENTS

The authors would like to thank the anonymous referee for his/her helpful comment. HML is supported by KRF grant No. 2006-341-C00018.

REFERENCES

Aarseth S. J., 1999, PASP, 111, 1333
Ardi E., Mineshige S., Spurzem R., 2005, JKAS, 38, 207
Baumgardt H., 2001, MNRAS, 325, 1323
Berczik P., Merritt D., Spurzem R., Bischof H. P., 2006, ApJ, 642, 21
Binney J., Tremaine S., 1987, Galactic Dynamics. Princeton Univ. Press, Princeton, NJ
Boily C. M., 2000, in Lancon A., Boily C. M., eds, ASP Conf. Ser. Vol. 211, Massive Stellar Clusters. Astron. Soc. Pac., San Francisco, p. 190
Boily C. M., Spurzem R., 2000, in Noels A., Magain P., Caro D., Jehin E., Parmetier G., Thoul A. A., eds, Proc. of the 35th Liege Intern. Astroph. Colloq. The Galactic Halo: From Globular Clusters to Field Stars, p. 607
Cohn H., 1980, ApJ, 242, 765
Drukier G. A., Fahlman G. G., Richer H. B., 1992, ApJ, 386, 106
Einsel C., Spurzem R., 1999, MNRAS, 302, 81 (Paper I)
Ernst A., Glaschke P., Fiestas J., Just A., Spurzem R., 2007, MNRAS, 377, 465
Fiestas J., Spurzem R., Kim E., 2006, MNRAS, 373, 677
Freitag M., Benz W., 2001, A&A, 375, 711
Freitag M., Rasio F. A., Baumgardt H., 2006, MNRAS, 368, 121
Fukushige T., Makino J., Kawai A., 2005, PASJ, 57, 1009
Giersz M., 1998, MNRAS, 298, 1239
Giersz M., Heggie D. C., 1994a, MNRAS, 268, 257
Giersz M., Heggie D. C., 1994b, MNRAS, 270, 298
Giersz M., Heggie D. C., 1997, MNRAS, 286, 709
Giersz M., Spurzem R., 1994, MNRAS, 269, 241
Goodman J., 1983, PhD thesis, Princeton Univ.
Goodman J., 1987, ApJ, 313, 576
Harfst S., Gualandris A., Merritt D., Spurzem R., Portegies Zwart S., Berczik P. 2007, New Astron., 12, 357
Hénon M. H., 1971, Ap&SS, 14, 151
Iwasawa M., Funato Y., Makino J., 2006, ApJ, 651, 1059
Joshi K. J., Rasio F. A., Portegies Zwart S., 2000, ApJ, 540, 969
Khalisi E., Amaro-Seoane P., Spurzem R., 2007, MNRAS, 374, 703
Kim E., 2003, PhD thesis, Seoul National Univ.
Kim E., Einsel C., Lee H. M., Spurzem R., Lee M. G., 2002, MNRAS, 334, 310 (Paper II)
Kim E., Lee H. M., Spurzem R., 2004, MNRAS, 351, 220 (Paper III)
Kustaanheimo P., Stiefel E., 1965, J. Reine Angew. Math., 218, 204
Lee H. M., Goodman J., 1995, ApJ, 443, 109L
Lee H. M., Ostriker J. P., 1987, ApJ, 322, L123
Lee K. H., Lee H. M., Sung H., 2006, MNRAS, 367, 646
Lupton R. H., Gunn J. E., 1987, AJ, 93, 1106
Makino J., Fukushige T., Koga M., Namura K., 2003, PASJ, 55, 1163
Makino J., Funato Y., 2004, ApJ, 602, 93
Makino J., Taiji M., 1998, Scientific Simulations with Special-Purpose Computers–the GRAPE Systems. Wiley VCH
Mikkola S., Aarseth S. J., 1990, CeMDA, 47, 375
Mikkola S., Aarseth S. J., 1993, CeMDA, 57, 439
Mikkola S., Aarseth S. J., 1996, CeMDA, 64, 197
Mikkola S., Aarseth S. J., 1998, New Astron., 3, 309
Spitzer L. J., Hart M. H., 1971, ApJ, 166, 483
Spitzer L., Jr., Mathieu R. D., 1980, ApJ, 241, 618
Spurzem R., Aarseth S. J., 1996, MNRAS, 282, 19S
Spurzem R., Giersz M., Takahashi K., Ernst A., 2005, MNRAS, 364, 948
Takahashi K., 1995, PASJ, 47, 561
Takahashi K., 1996, PASJ, 48, 691
Takahashi K., 1997, PASJ, 49, 547
Takahashi K., Lee H. M., 2000, MNRAS, 316, 617
Takahashi K., Portegies Zwart S. F., 1998, ApJ, 503, L49
Takahashi K., Portegies Zwart S. F., 2000, ApJ, 535, 759
Yim K., Lee H. M., 2002, JKAS, 35, 75Y

This paper has been typeset from a TEX/LATEX file prepared by the author.